This method was shown to provide substantial model reduction (two orders of magnitude) without significant loss of accuracy for representative aerodynamic and aeroelastic problems. Unlike the eigensystem approach to reduced-order modeling, which discards states based on modal damping, balanced model reduction discards states that provide little contribution to the system output. This criterion yields better performance for both transient and long time response.

A physical interpretation of the first few balanced states suggests that the optimal basis vectors are composed of solutions to simple, exact problems. Two examples shown here related transient response to a flat plate either descending or rotating with no mean flow. Such limiting-case behavior may serve as a guide in finding balanced states of more complex configurations.

The algorithm employed to calculate the appropriate balancing transformation carries the same computational cost as an eigenvalue decomposition, which is proportional to system size cubed. Thus, as problem size grows, direct calculation of the balancing transformation becomes infeasible. Special algorithms, similar to the Lanczos algorithm for finding the dominant eigenvectors and eigenvalues of very large systems, will be necessary to find the dominant balanced coordinates at reasonable cost. It is believed that the physical insight provided by the simple cases discussed here will provide a solid starting point for such algorithm development.

Acknowledgments

The authors thank Earl Dowell and Kenneth Hall for their insightful comments on reduced-order modeling techniques as applied to aerodynamic systems.

References

[1]Holmes, P., Lumley, J. L., and Berkooz, G., *Turbulence, Coherent Structures, Dynamical Systems and Symmetry*, Cambridge Univ. Press, Cambridge, England, U.K., 1996.

[2]Breuer, K. S., and Sirovich, L., "The Use of the Karhunen–Loève Procedure for the Calculation of Linear Eigenfunctions," *Journal of Computational Physics*, Vol. 96, 1991, pp. 277–296.

[3]Gordeyev, S. V., and Thomas, F. O., "Coherent Structure in the Turbulent Planar Jet. Part 1. Extraction of Proper Orthogonal Decomposition Eigenmodes and Their Self-Similarity," *Journal of Fluid Mechanics*, Vol. 414, 2000, pp. 145–194.

[4]Dowell, E. H., Hall, K. C., and Romanowski, M. C., "Eigenmode Analysis in Unsteady Aerodynamics: Reduced Order Models," *Applied Mechanics Review*, Vol. 50, No. 6, 1997, pp. 371–386.

[5]Hall, K. C., "Eigenanalysis of Unsteady Flows About Airfoils, Cascades, and Wings," *AIAA Journal*, Vol. 32, No. 12, 1994, pp. 2426–2432.

[6]Hall, K. C., Florea, R., and Lanzkron, P. J., "A Reduced Order Model of Unsteady Flows in Turbomachinery," *Journal of Turbomachinery*, Vol. 117, July 1995, pp. 375–383.

[7]Florea, R., Hall, K. C., and Cizmas, P. G. A., "Reduced-Order Modeling of Unsteady Viscous Flows in a Compressor Cascade," *AIAA Journal*, Vol. 36, No. 6, 1998, pp. 1039–1048.

[8]Baker, M., "Model Reduction Of Large, Sparse, Discrete Time Systems with Application To Unsteady Aerodynamics," Ph.D. Dissertation, Dept. of Mechanical and Aerospace Engineering, Univ. of California, Los Angeles, 1996.

[9]Baker, M. L., Mingori, D. L., and Goggin, P. J., "Approximate Subspace Iteration for Constructing Internally Balanced Reduced Order Models of Unsteady Aerodynamic Systems," *AIAA Structures, Structural Dynamics and Materials Conference*, AIAA, Reston, VA, 1996, pp. 1070–1085.

[10]Kailath, T., *Linear Systems*, Prentice–Hall, Englewood Cliffs, NJ, 1980, pp. 609–619.

[11]Skogestad, S., and Postlewaite, I., *Multivarible Feedback Control*, Wiley, Chichester, England, U.K., 1996.

[12]Theodorsen, T., "General Theory of Aerodynamic Instability and the Mechanism of Flutter," NACA TR 496, 1935.

[13]Laub, A. J., Heath, M. T., Paige, C. C., and Ward, R. C., "Computation of System Balancing Transformations and Other Applications of Simultaneous Diagonalization Algoriths," *IEEE Transactions on Automatic Control*, Vol. AC-32, No. 1, 1987, pp. 115–122.

[14]Gudmundsson, T., and Laub, A. J., "Approximate Solution of Large Sparse Lyapunov Equations," *IEEE Transactions on Automatic Control*, Vol. 39, No. 5, 1994, pp. 1110–1114.

A. Plotkin
Associate Editor

Effect of the Vortex Whistle on the Discharge Coefficient of Orifices

A. Jocksch*
ETH Zürich, CH-8092 Zurich, Switzerland
and
C. P. Gravett†
Rolls–Royce, plc.,
Derby, England DE24 8BJ, United Kingdom

Nomenclature

A	=	cross-sectional area
C_D	=	discharge coefficient
d	=	orifice diameter
m	=	actual mass flow rate
m_{th}	=	theoretical mass flow rate
P	=	total pressure
p	=	static pressure
Q	=	mass flow function
R	=	gas constant
Re	=	Reynolds number
T	=	temperature
t	=	orifice thickness
γ	=	ratio of specific heats

Introduction

IN the literature, discharge coefficients scatter widely for square-edged orifices, where the orifice thickness is similar to the orifice diameter. The physics of this uncertainty has been subject of discussion. Lichtarowicz et al.[1] investigated incompressible flow through such orifices. In the case of a thickness-to-diameter ratio of $t/d = 1/2$, two different flow regimes were identified. A hysteresis in the discharge coefficient was presumed to exist. Other experiments showed a train of vortex rings at certain low Reynolds numbers.[2] Hay and Spencer[3] also measured different discharge coefficients for the same arrangement. By the referencing of their measurements with compressible flow, Deckker and Chang[4] identified a hysteresis in discharge coefficients with respect to the pressure ratio at $t/d = 1/2$. When steady flow was assumed, the hysteresis effect was explained as to be the result of reattachment and nonreattachment of the flow to the orifice.[2,4]

When it is considered that flow through an orifice can generate sound,[5] it is shown that the discharge coefficient is influenced by an acoustical phenomenon, the socalled vortex whistle, a self-induced unsteadiness driven by feedback oscillations. Numerical simulations have been produced that connect this phenomenon to the discharge coefficient hysteresis mentioned earlier.

Discharge Through Orifices

The discharge coefficient is defined as the ratio of the actual mass flow rate m to the theoretical mass flow rate for isentropic flow m_{th}:

$$C_D = m/m_{\text{th}} \tag{1}$$

Received 3 June 2002; revision received 16 May 2003; accepted for publication 14 November 2003.

*Ph.D. Student, Institute of Fluid Dynamics, Sonneggstrasse 3; jocksch@ifd.mavt.ethz.ch.

†Fluid Systems Team Leader, Trent Hall 1, P.O. Box 31.

where the theoretical mass flow rate is

$$m_{\text{th}} = QAP\Big/\sqrt{T} \tag{2}$$

When the pressure ratio is less than or equal to the choking pressure ratio, the mass flow function is determined by

$$Q^2 = (2/R)[\gamma/(\gamma-1)]\left[1-(P/p)^{(1-\gamma)/\gamma}\right](P/p)^{-2/\gamma} \tag{3}$$

The orifice pressure ratio P/p is defined as the total pressure upstream of the orifice divided by the static pressure downstream of the orifice. Beyond the choking pressure ratio ($P/p_{\text{cho}} = 1.893$ for $\gamma = 1.4$), the mass flow function remains constant at the choking value. Only Reynolds numbers higher than $Re > 2 \times 10^4$ have been considered. In this case, the influence of the Reynolds number on the discharge coefficient becomes negligible.[3]

For steady flow, there are different flow patterns depending on the thickness-to-diameter ratio of the orifice.[2] For a thin orifice plate, the jet contracts to the smallest cross-sectional area downstream of the orifice, the so-called vena contracta. A toroidal vortex starting at the orifice plate is formed around the jet. When the thickness of the orifice plate becomes larger, the expansion after the vena contracta is limited by the orifice bore, that is, by reattachment of the flow to the wall of the bore. Hence, one toroidal vortex originates at the inlet edge, and a second one forms at the downstream edge of the orifice. Both enclose the jet in their center. The transitional region has been considered in a marginally separated and a marginally reattached flow regime.[2]

In addition to the steady-state flow conditions, it is also known that under certain conditions flow may produce a vortex whistle when the orifice diameter is comparable to the plate thickness.[5] It is produced when the edge at the orifice entrance serves as vortex generator and the edge at the bore exit serves as the vortex receiver. Every vortex passing the outlet of the orifice induces a sound wave that travels back through the bore of the orifice and separates the next vortex when it reaches the inlet.

Numerical Simulations

Numerical simulations have been performed using FLUENT[6] with a two-dimensional axisymmetric model using the k–ε, Reynolds-stress (RS) and Spalart–Allmaras (SA) turbulence models (see Ref. 7). Pipes of three times the orifice diameter are attached upstream and downstream of the orifice. This ensures a negligible approach velocity. The lengths of the inlet and outlet are 5 and 30 orifice diameters, respectively. The influence of inflow and outflow boundary conditions is thereby minimized. A structured mesh with 5757 cells and local mesh refinement was used (Fig. 1). Further characteristics of the compressible simulations are pressure inlet and pressure outlet boundary conditions[6] and wall functions.

To test the accuracy of the model, the zero orifice plate thickness model results were compared to the standard International Organization for Standardization–American Society of Mechanical Engineers (ISO–ASME) discharge nozzle characteristics for flow meters adapted for compressibility effects[8] (Fig. 2a). The simulated discharge coefficients match the values delivered from the ISO–ASME formula very well. This applies to all three turbulence models considered.

Unlike steady-state flow for the zero length orifice, for $t/d = 1/2$ different turbulence models deliver different results. The RS turbulence model delivers two flow regimes, steady-state flow (Fig. 3a) at

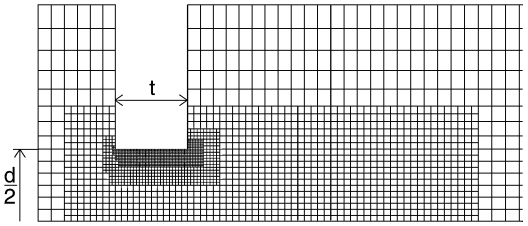

Fig. 1 Section of the axisymmetric mesh showing three levels of local mesh refinement around the orifice plate.

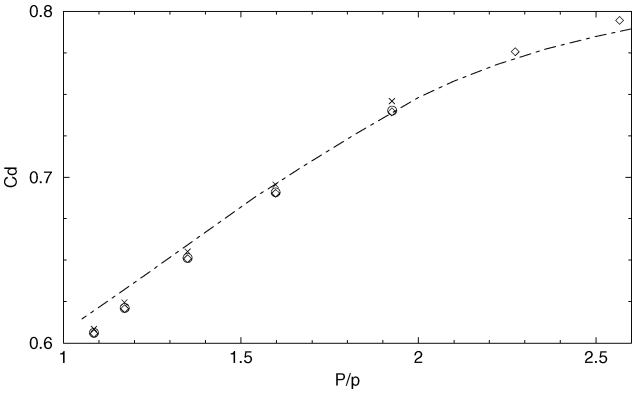

a) Zero thickness orifice plate

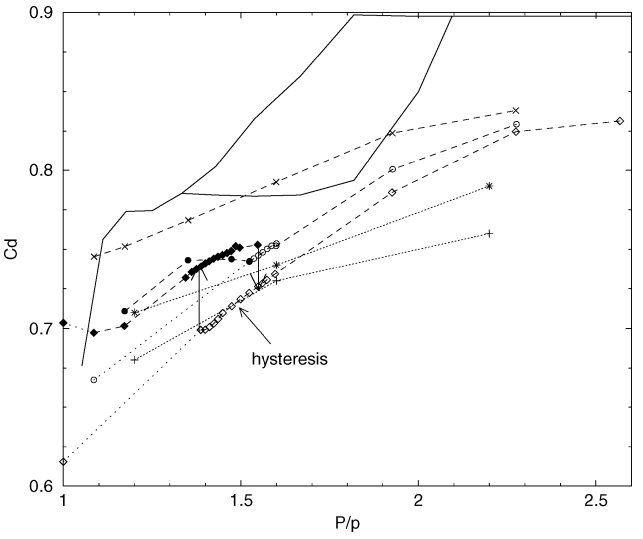

b) Thickness to diameter ratio of orifice plate $t/d = 1/2$

Fig. 2 Discharge coefficients calculated with turbulence models: ×, k–ε; ◇, RS; ◆, RS vortex shedding; ○, SA; and ●, SA vortex shedding compared to reference values: — · —, ISO–ASME discharge nozzle (adapted)[8]; ——, Deckker and Chang[4]; +, Hay and Spencer[3] series 1; and ∗, Hay and Spencer[3] series 2.

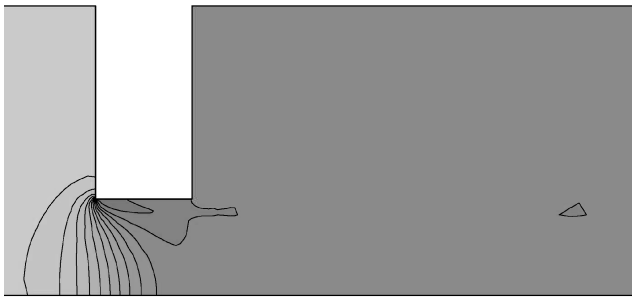

a) Steady-state flow

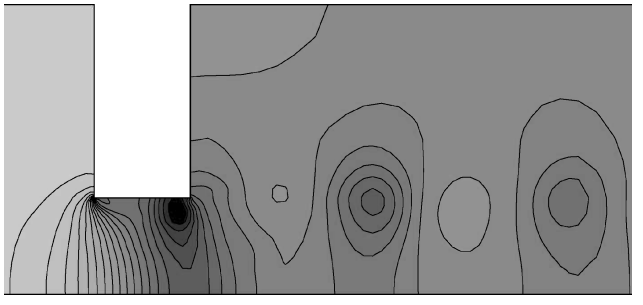

b) Vortex shedding, instantaneous

Fig. 3 Qualitative static pressure contours Reynolds-stress turbulence model $l/d = 1/2$ and $P/p = 1.345$: dark colors correspond to low pressure.

high-pressure ratios and vortex shedding (Fig. 3b) at low-pressure ratios with hysteresis for the discharge coefficient (Fig. 2b). The SA turbulence model also gives both flow regimes, but without the hysteresis, and the flow becomes steady again at low-pressure ratios. The k–ε turbulence model does not predict any vortex shedding. Transient boundary conditions were used changing P/p in steps of $0.01 \cdot p$ in the hysteresis region. Almost all simulated values are within the range of the different experimental data sets from Refs. 3 and 4. Note that the measured discharge coefficients from Ref. 3 appear to be overestimated by 4–5% (Ref. 8). The vortex shedding flow regime shows higher discharge coefficients than steady-state flow.

Simulations for incompressible flow were made using pipes with four times the orifice diameter and a finer mesh at $Re = 1.028 \times 10^5$. Vortex shedding is suppressed for a constant mass flow rate by prescribing the velocity at the inlet. The discharge coefficients for the incompressible case (Fig. 2b, $P/p = 1$) match the compressible numerical results well.

A mesh refinement by quadrupling cells for the zero length orifice with RS turbulence model at $P/p = 1.074$ increases the discharge coefficient by 0.5%. Taking a 10 times smaller time step for $l/d = 1/2$ for the RS turbulence model at $P/p = 1.074$ increases the discharge coefficient by less than 1%. In contrast to the zero length orifice, the wide variation of the results for $t/d = 1/2$ for different turbulence models indicates the limitation of the numerical method for modeling this configuration. However, the results of the RS turbulence model seem to replicate the physics of the arrangement qualitatively. They confirm the hysteresis in the discharge coefficient and the vortex whistle mechanism.

Whether the pipe geometry has a significant influence on the discharge coefficient with respect to resonances needs to be examined. However, the vortex shedding for the incompressible simulation, where resonances cannot be taken into account, indicates that this is not the case.

Conclusions

It has been shown that the hysteresis observed previously can be explained by the transition between two flow regimes, which are defined by steady-state flow at high-pressure ratios and vortex shedding at low-pressure ratios. Because the vortex shedding is part of the vortex whistle mechanism, the hysteresis effect is linked to this phenomenon.

The results are consistent with the initial observations, which include a hysteresis, a train of vortex rings, and a vortex whistle. Transitions between the two flow regimes, that is, separated flow and reattached flow, with a hysteresis[2] cannot be confirmed.

Acknowledgments

Simulations have been performed during a placement of the first author at Rolls–Royce, plc. Ansty, England, United Kingdom. The authors thank B. Whinray, D. Livingstone, G. D. Snowsill, J. P. Kunsch, and S. Schlamp for their help and advice.

References

[1]Lichtarowicz, A., Duggins, R. K., and Markland, E., "Discharge Coefficients for Incompressible, Noncavitating Flow Through Long Orifices," *Journal of Mechanical Engineering Science*, Vol. 7, No. 2, 1965, pp. 210–219.

[2]Ward-Smith, A. J., *Pressure Losses in Ducted Flows*, Butterworths, London, 1971, pp. 135–157.

[3]Hay, N., and Spencer, A., "Discharge Coefficients of Cooling Holes with Radiused and Chamfered Inlets," *Journal of Turbomachinery*, Vol. 114, No. 4, 1992, pp. 701–706.

[4]Deckker, B. E. L., and Chang, Y. F., "An Investigation of Steady Compressible Flow Through Thick Orifices," *Thermodynamics and Fluiddynamics Convention 1966*, Vol. 180, Pt. 3J, Institution of Mechanical Engineers, London, 1966, pp. 312–323.

[5]Morse, P. M., and Ingard, K. U., *Theoretical Acoustics*, Princeton Univ. Press, Princeton, NJ, 1968, pp. 755–758.

[6]"FLUENT5 User's Guide," Fluent, Inc., Lebanon, NH, July 1998.

[7]Rayer, Q. G., and Snowsill, G. D., "Validation of FLUENT Against Incompressible and Compressible Flow Through Orifices," *CFD in Fluid Machinery Design*, Professional Engineering Publishing, Bury St. Edmunds, England, U.K., 1998, pp. 79–91.

[8]Parker, D. M., and Kercher, D. M., "An Enhanced Method to Compute the Compressible Discharge Coefficient of Thin and Long Orifices with Inlet Corner Radiusing," *Heat Transfer in Gas Turbine Engines*, Vol. 188, American Society of Mechanical Engineers, New York, 1991, pp. 53–63.

K. N. Ghia
Associate Editor

Low-Temperature Effects on E-Glass/Urethane at High Strain Rates

Shunjun Song* and Jack R. Vinson†
University of Delaware, Newark, Delaware 19716
and
Roger M. Crane‡
U.S. Naval Surface Warfare Center, West Bethesda, Maryland 20817-5700

Introduction

COMPOSITE materials are used in a wide variety of low-temperature applications because of their unique and highly tailorable properties. These low-temperature applications of composites include their use in arctic environments and most of them involve dynamic loads. According to the U.S. Navy, under certain conditions naval vessels may encounter strain rate up to 1200/s. Because the dynamic properties of composite materials may vary widely with strain rate, it is important to use these dynamic properties in design when the loading conditions require it.

All too few materials have been characterized both at high strain rates and at low temperature. Still less effort has been spent in trying to model the high strain rate properties to develop a predictive capability. It has been hoped that earlier modelings for metals, such those as Johnson and Cook[1] and Zerilli and Armstrong[2] might be used for composite materials. The Johnson–Cook model was modified by Weeks and Sun[3] for composite materials. Other recent modeling and research have been performed by Thiruppukuzhi and Sun,[4] Hsiao et al.[5] and Tsai and Sun.[6] Vinson and Woldesenbet[7] have characterized the high strain rate and fiber orientation effects on one typical graphite/epoxy composite. Most of these characterizations model ultimate strengths only.

Over the last several years a program has been conducted to determine experimentally the dynamic compressive material properties of various composite materials that are of interest to industry and to various government agencies. A split Hopkinson pressure bar was used for all of these compression experiments. In all cases, at least three replicate specimens were tested, and subsequently the data was analyzed to determine both mean values and standard deviations. Those experiments were conducted at room temperature, and the results are presented in Refs. 8–18. The mean values of those data[8–18] were presented recently in Ref. 19, where polynomial expressions for the ultimate strengths and moduli of elasticity were

Received 17 July 2002; revision received 14 October 2003; accepted for publication 3 November 2003.

*Research Assistant, Department of Mechanical Engineering; currently Ph.D. Candidate, Department of Aerospace Engineering, University of Michigan, Ann Arbor, MI 48109. Student Member AIAA.

†H. Fletcher Brown Professor, Department of Mechanical and Aerospace Engineering; vinson@me.udel.edu. Fellow AIAA.

‡Composite Materials Section Head, Carderock Division.